Electronic supplementary information for

Design and in-situ synthesis of hierarchical SAPO-34@kaolin composites as catalysts for methanol to olefins

Lina Zhang, ‡[a] Haiyan Liu, ‡[a] Yuanyuan Yue, [b] Unni Olsbye, [c] and Xiaojun Bao, [ab*]

[a]*State Key Laboratory of Heavy Oil Processing, China University of Petroleum, Beijing 102249, P. R. China*

[b]*National Engineering Research Center of Chemical Fertilizer, College of Chemical Engineering, Fuzhou University, Fuzhou 350116, P. R. China*

[c]*Center for Materials Science and Nanotechnology, Institute of Chemistry, University of Oslo, P.O. Box Blindern, N-0315 Oslo, Norway*

[*]*Corresponding author: baoxj@fzu.edu.cn (X. Bao)*

Table of contents

1. Supplementary Table

Table S1. Compositions of the raw KMS and the active SiO_2, Al_2O_3, and P_2O_5 contents of the thermally treated KMS.

Content (wt.%)	Raw KMS[a]	Thermally treated KMS at different temperatures			
		600 °C[b]	700 °C[b]	800 °C[b]	900 °C[b]
SiO_2	48.6	0.8	3.5	2.6	3.0
Al_2O_3	44.6	19.4	37.7	30.2	11.9
P_2O_5	0.3	0.0	0.3	0.1	0.3
SiO_2/Al_2O_3 (mol/mol)	-	0.08	0.16	0.15	0.43
P_2O_5/Al_2O_3 (mol/mol)	-	0.000	0.006	0.002	0.020

Notes: [a] The composition of the raw KMS was analyzed by XRF; [b] the contents of active SiO_2, Al_2O_3, and P_2O_5 were quantified by ICP-AES.

Table S2. Deconvolution results of the ^{29}Si MAS NMR spectra of S@KMS, S@KMS-C, and S@KMS-CT based on the normalized peak areas of the different Si species.

Sample	SAPO domain	SA domain				
	Si(4Al) (%)	Si(4Al) (%)	Si(3Al, 1Si) (%)	Si(2Al, 2Si) (%)	Si(1Al, 3Si) (%)	Si(4Si) (%)
S@KMS	8.66	4.97	8.94	15.48	27.32	34.63
S@KMS-C	8.90	3.87	10.10	14.86	38.03	24.23
S@KMS-CT	9.04	5.52	12.74	14.03	32.38	26.29

2. Supplementary Figures

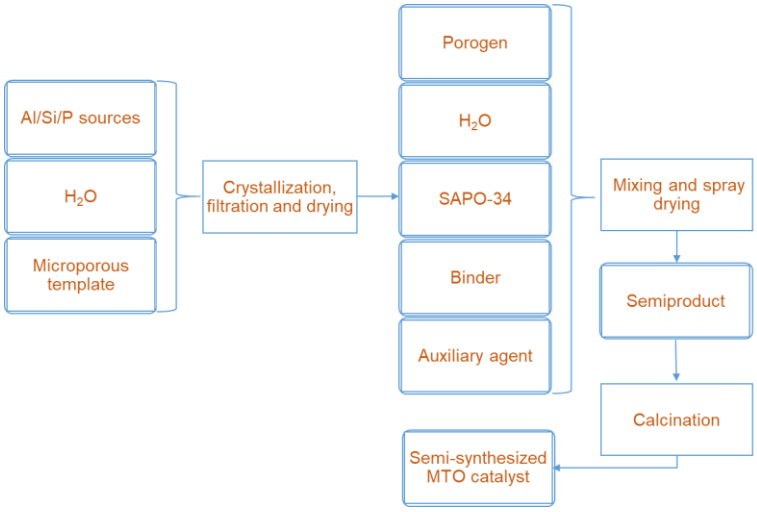

Fig. S1. Semi-synthesis of SAPO-34 based MTO catalyst.[1]

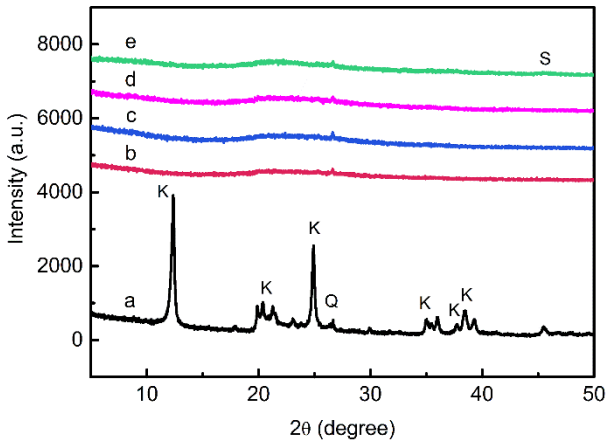

Fig. S2. XRD patterns of the raw KMS (a) and the KMS thermally activated at 600 ºC (b), 700 ºC (c), 800 ºC (d), and 900 ºC (e). K, Q, and S denote kaolinite, quarts, and spinel, respectively.

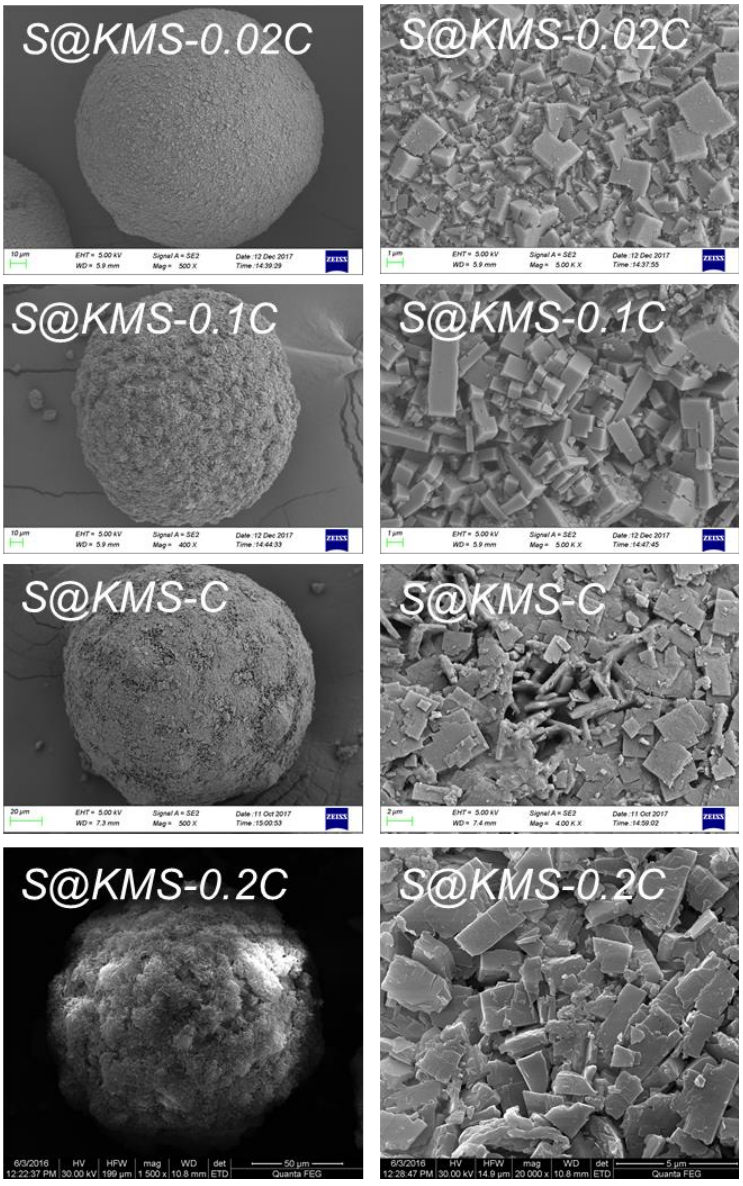

Fig. S3. SEM images of the samples synthesized with different amounts of CTAB.

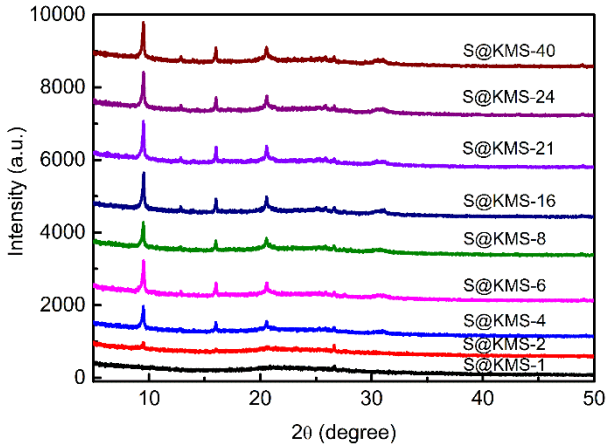

Fig. S4. XRD patterns of S@KMS-x (x denotes crystallization time) obtained after crystallization for different lengths of time without any surfactant.

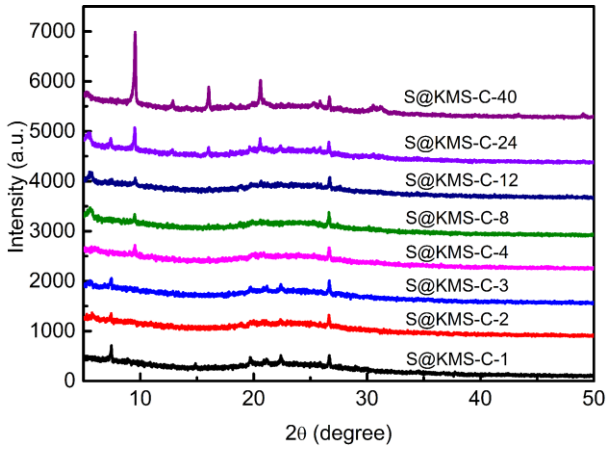

Fig. S5. XRD patterns of S@KMS-C-x (x denotes crystallization time) obtained after crystallization for different lengths of time in the presence of CTAB.

Fig. S6. The image of the two mixtures (K-W and K-W-C) after agitation at 200 °C for 3 h.

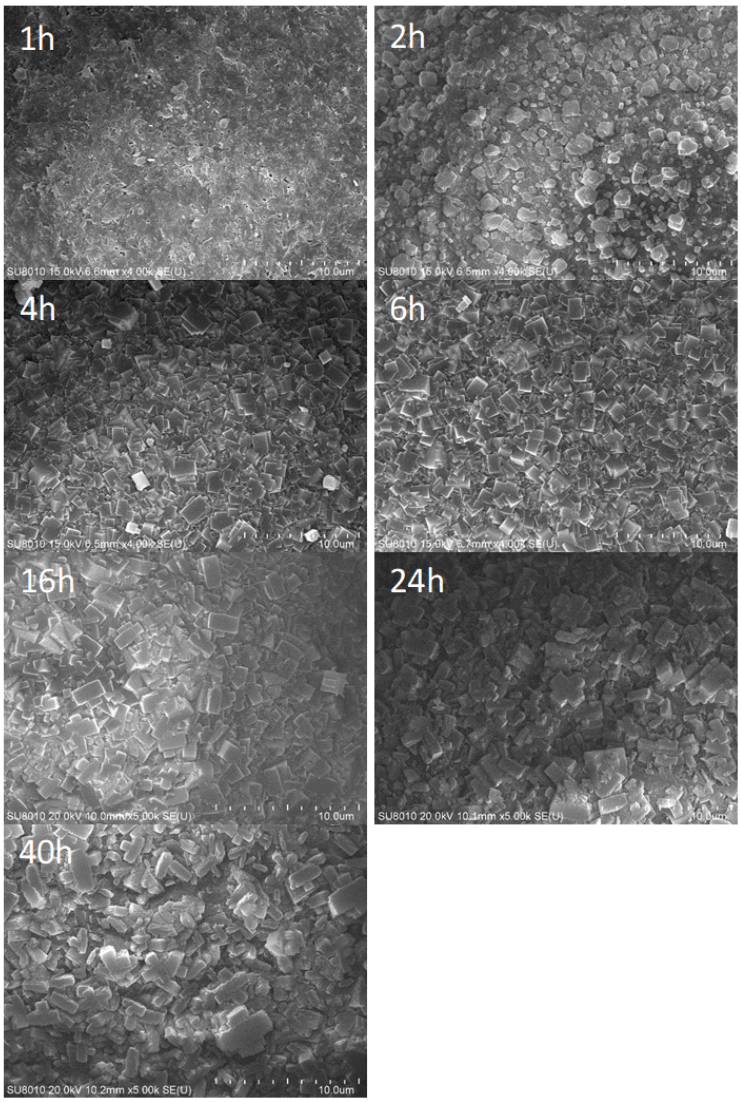

Fig. S7. SEM images of the samples obtained after crystallization for different lengths of time without the involvement of any surfactant: S@KMS-1, S@KMS-2, S@KMS-4, S@KMS-6, S@KMS-16, S@KMS-24, and S@KMS-40.

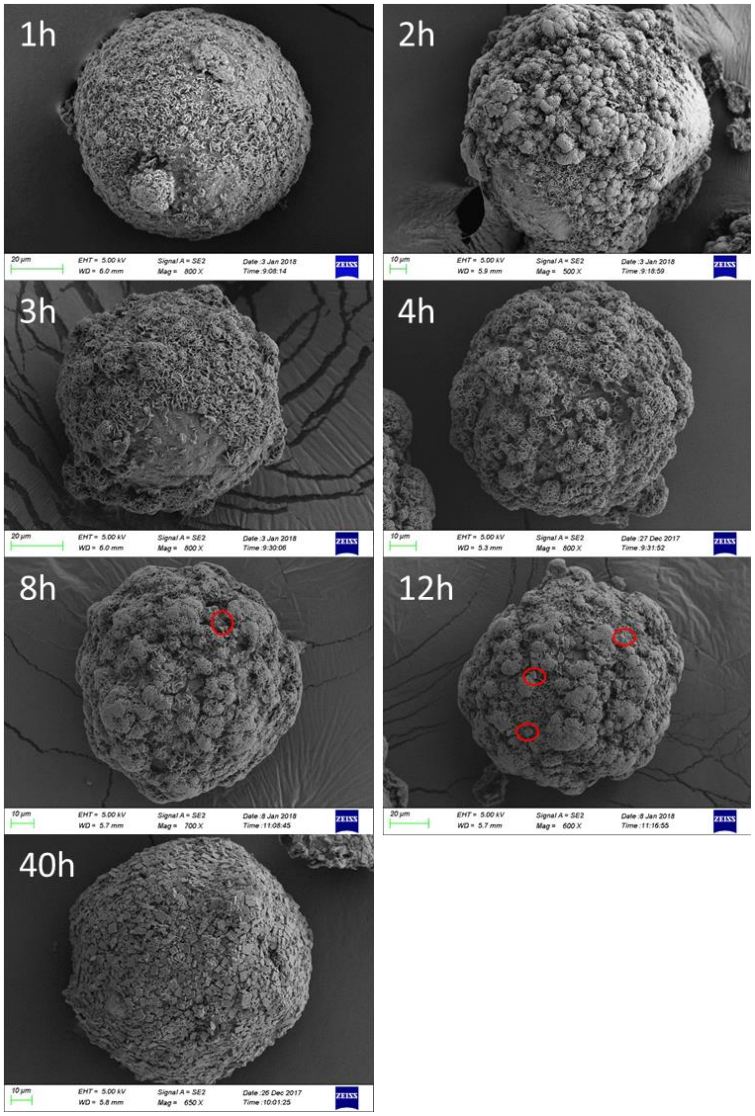

Fig. S8. SEM images of the samples obtained after crystallization for different lengths of time in the presence of CTAB: S@KMS-C-1, S@KMS-C-2, S@KMS-C-3, S@KMS-C-4, S@KMS-C-8, S@KMS-C-12, and S@KMS-C-40.

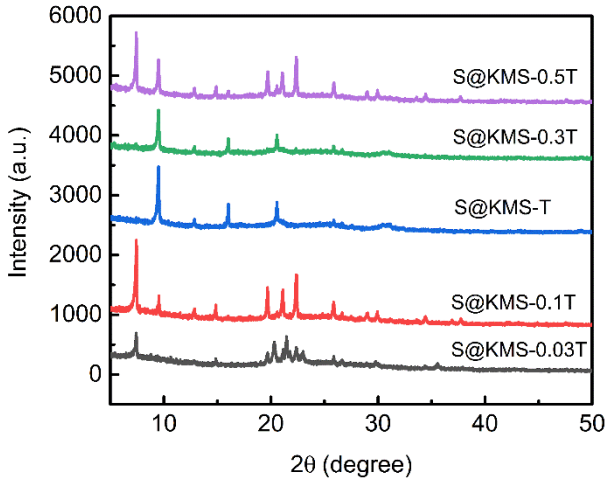

Fig. S9. XRD patterns of the samples synthesized with different amounts of TPOAC.

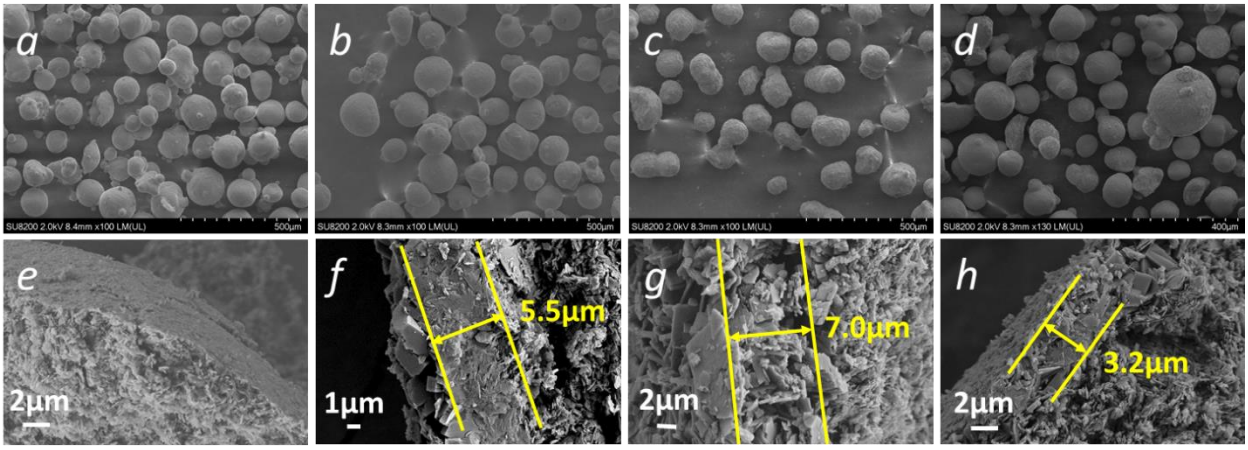

Fig. S10. The overall and cross-sectional SEM images of KMS (a and e), S@KMS (b and f), S@KMS-C (c and g), and S@KMS-CT (d and h).

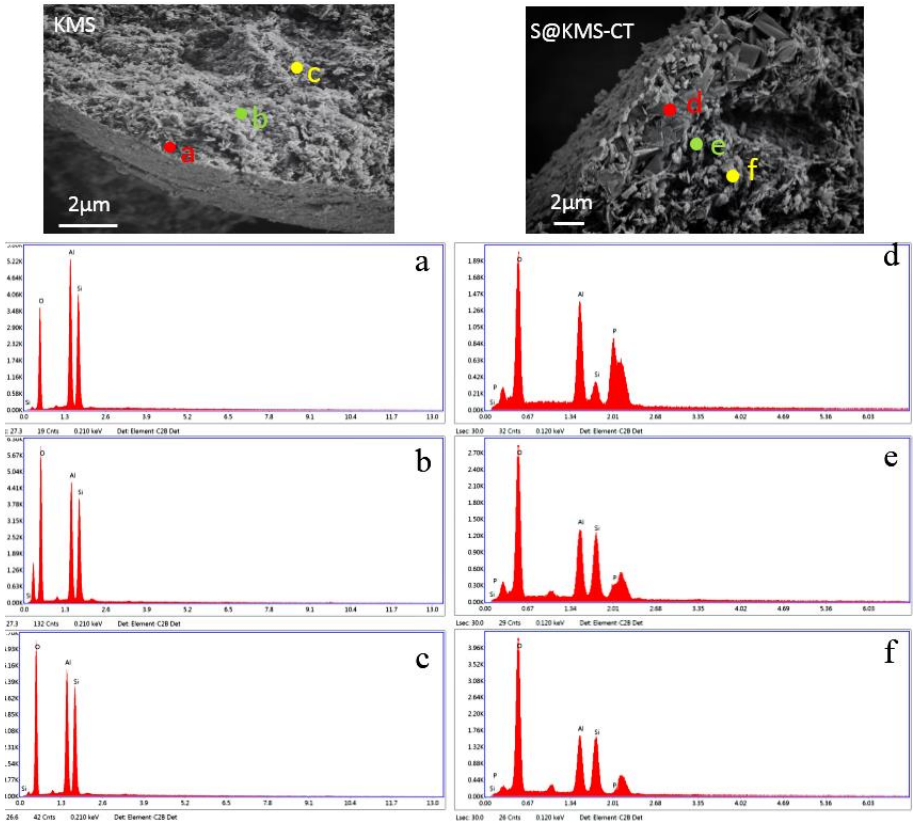

Fig. S11. The cross-sectional EDS analysis results of the KMS and S@KMS-CT at (a) spot a, (b) spot b, (c) spot c, (d) spot d, (e) spot e, and (f) spot f.

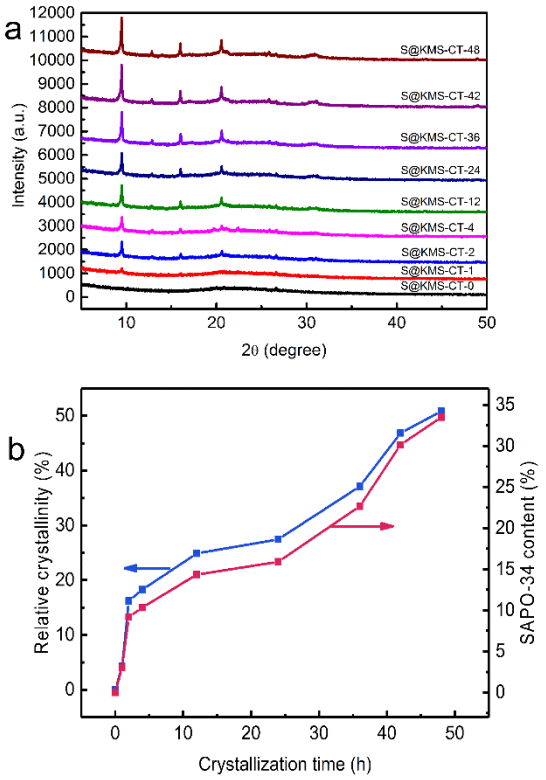

Fig. S12. XRD patterns (a) and corresponding relative crystallinities and SAPO-34 contents of the samples (b) obtained after crystallization for different lengths of time with the involvement of both CTAB and TPOAC.

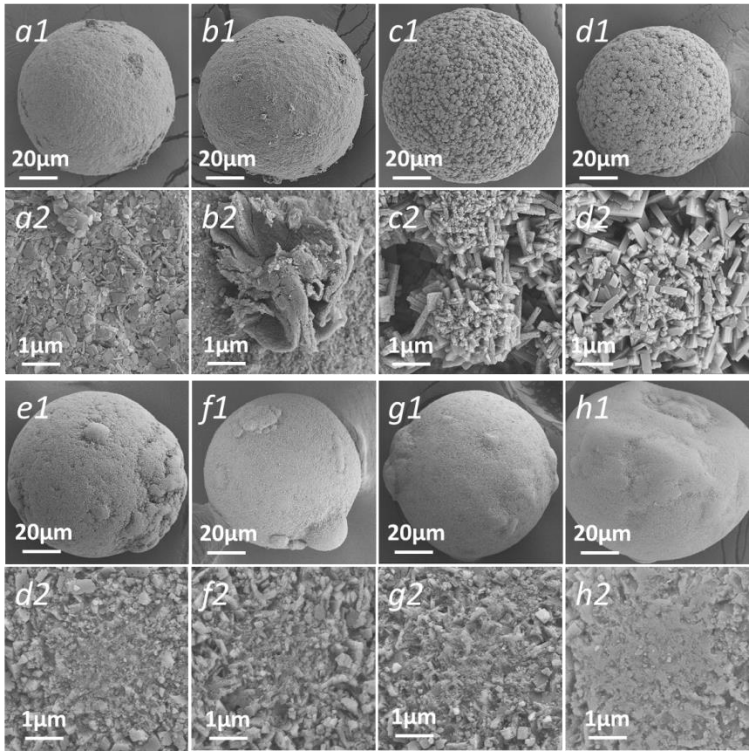

Fig. S13. SEM images of the samples obtained after crystallization for different lengths of time with the simultaneous involvement of CTAB and TPOAC: S@KMS-CT-0 (a1, a2), S@KMS-CT-1 (b1, b2), S@KMS-CT-2 (c1, c2), S@KMS-CT-4 (d1, d2), S@KMS-CT-12 (e1, e2), S@KMS-CT-24 (f1, f2), S@KMS-CT-36 (g1, g2), and S@KMS-CT-42 (h1, h2).

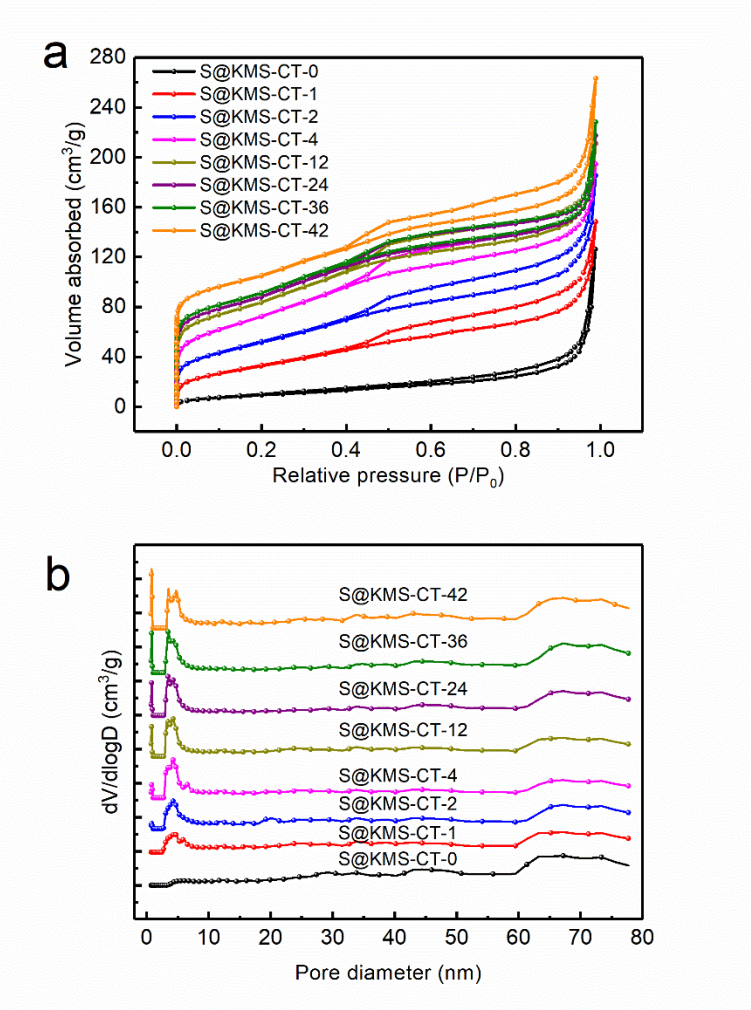

Fig. S14. N_2 adsorption-desorption isotherms (a) and the corresponding NDFT pore size distributions of the S@KMS-CT-x samples (b) obtained after crystallization for different lengths of time.

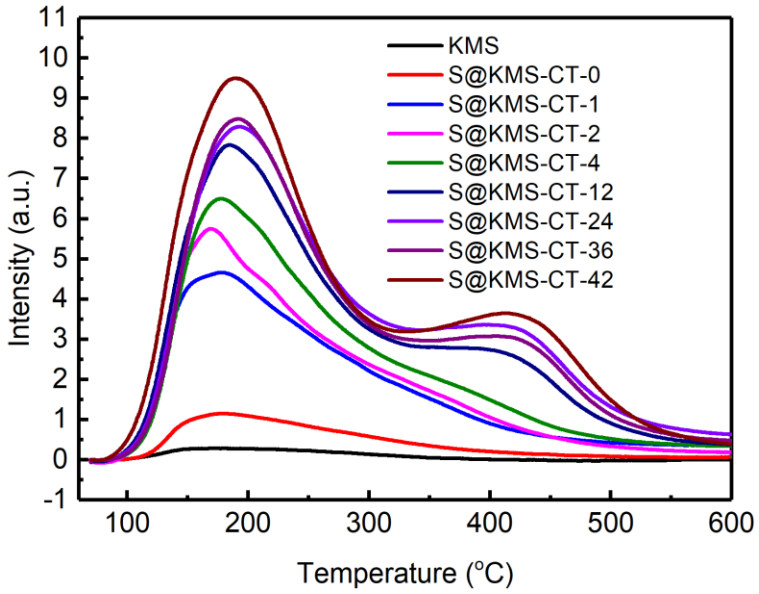

Fig. S15. NH_3-TPD curves of the samples synthesized after crystallization for different lengths of time with the involvement of both CTAB and TPOAC.

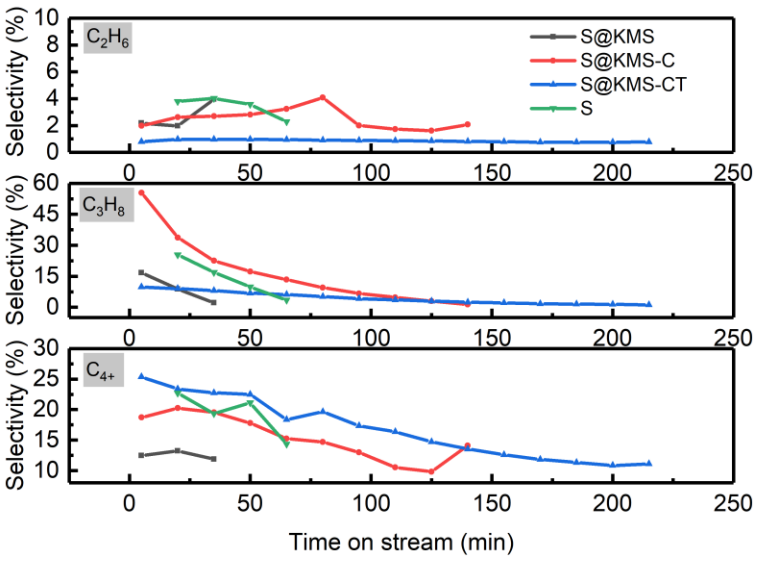

Fig. S16. Selectivity to C_2H_6, C_3H_8, and $C4^+$ over S@KMS, S@KMS-C, S@KMS-CT, and S (reaction conditions: 450 ºC, WHSV = 2.5 h^{-1}, and 95 wt.% aqueous methanol solution).

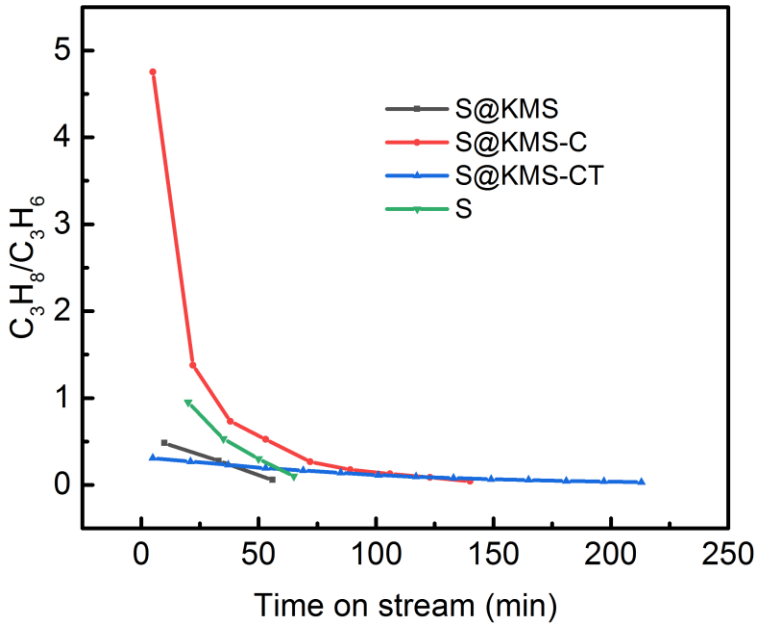

Fig. S17. Hydrogen transfer indexs (HTIs C_3H_8/C_3H_6) values of methanol conversion over S, S@KMS, S@KMS-C, and S@KMS-CT.

3. References

1. P. Tian, Y. Wei, M. Ye and Z. Liu, *ACS Catal.*, 2015, **5**, 1922-1938.